Master thesis

Electron positron annihilation into photons at NNLO accuracy

by

Luca Naterop

at the

Department of Physics
University of Zurich

Supervisors

Prof. Dr. Adrian Signer
Dr. Yannik Ulrich
Tim Engel

June 2021

Abstract

In this master thesis we present a high-precision QED calculation for the process $e^+e^- \to 2\gamma$, a process relevant in light of the PADME experiment at INFN. The accuracy of the result, currently incorporating photonic contributions, is based on an exact NNLO calculation that includes effects of the electron's nonvanishing mass. For an observable that models the experimental cuts at the DAΦNE collider, we provide numerical results for the integrated cross section, as well as a number of relevant differential distributions. The process is implemented in the latest version of McMule, a unified framework for precision QED.

Acknowledgements

Throughout the work on this project, I have received a lot of inspiration and support. I would like to express my gratitude to Adrian Signer for suggesting the project and giving me the opportunity to work in this fascinating environment. Thanks also to Yannick Ulrich and Tim Engel for their invaluable day-to-day support. I am also thankful to Nigel Glover for providing the two-loop results and to Max Zoller for his help with OpenLoops.

Contents

1 Introduction

The Standard Model (SM) of particle physics has been able to successfully describe a wide range of observed phenomena [1]. The theory is capable of characterizing three out of the four fundamental interactions in the universe, as well as classifying the whole set of observed elementary particles. Most SM processes can be accurately predicted through application of perturbation theory.
Even though the SM is a self-consistent theory and has proven successfully in providing predictions for experimental observables, it has a number of shortcomings [2]. It does not include the gravitational interaction and therefore cannot be considered a complete theory of the fundamental interactions in our universe. It does not account for the observed asymmetry between matter and antimatter [3] and it does not include neutrino masses as demonstrated by their oscillations [4].
It also does not contain any description of dark matter by means of a particle with the properties consistent with cosmological observations. Various evidence from astrophysical and cosmological observations suggest the existence of such a type of matter constituting about 85% of the matter content of the universe. It is implied for example by galactic rotation curves [5] and temperature fluctuations of the cosmic microwave background [6]. The lack of description for it within the SM is often considered to be a shortcoming of the theory, and naturally, many extensions thereof are being investigated [7].
A recently revived proposition for physics Beyond the Standard Model (BSM) is the dark photon, a hypothetical spin-1 particle arising from a minimal extension of the SM with a new $U(1)$ abelian gauge symmetry [8]. In this model, the dark photon serves as a portal through which it couples to ordinary charged particles, and could thus be detectable. Additional interest in the dark photon arises from its ability to explain the apparent variance in the magnetic moment of the muon [9], even though this seems to be disfavoured now.
In recent years, a lot of interest has been devoted to quantum chromodynamics (QCD) and the electroweak theory, which allow to predict processes at the high-energy frontier. Since the Large Hadron Collider (LHC) has begun to operate at the energy of $\sqrt{s} = 13$ TeV and no compelling evidence of BSM physics has been found, low-energy phyisics has become an ever more important alternative line of search [10] for new physics.
One notable low-energy experiment searching for BSM signatures is the PADME experiment (Positron Annihilation into Dark Matter Experiment) at Laboratori Nazionali di Frascati of INFN, whose objective is to search for dark matter by trying to unveil the dark sector of the SM [11] in an electron positron annihilation experiment. The experiment is designed to detect dark photons by measuring the missing invariant mass in the final state photons.
The present work aims at calculating the process $e^+e^- \to 2\gamma$ at next-to-next-to leading order (NNLO) accuracy, including effects of the electron's non-vanishing mass. This can help to accurately estimate the SM background of the process studied in the PADME experiment, ultimately allowing a finer comparison of experiment to theory. It can also be beneficial for determining luminosity at e^+e^- colliders, which has historically been done using Bhabha scattering [12], but could be done with $e^+e^- \to 2\gamma$, too.
In many respects, quantum electrodynamics (QED) is simpler than QCD and the electroweak theory because the interaction is based on an abelian $U(1)$ group in QED, where as QCD is based on the nonabelian $SU(3)$ group. However, in QED the logarithms that contain the fermion

masses are physical in the sense that they can be measured in experiments, and they can be large which can result in numerical instabilities. The need to account for the fermion mass thus introduces a challenge that is easily overlooked when one compares QED to QCD.
In Chapter 2, we discuss the methods that were employed in the calculation, where we first give a brief overview of the steps involved, followed by a more detailed discussion of some of the strategies employed. In Chapter 3, we give results for integrated cross sections and a number of differential distributions. Finally, a conclusion of the present work is given in Chapter 4, along with an outlook.

2 Methods

In [13, 14] the general methods for calculactions in quantum field theory (QFT) are introduced. The QED calculation performed in the present work can roughly be divided into the following steps:

1. We select a theory by writing down a Lagrangian. We choose QED, so

$$\mathcal{L} = -\frac{1}{4}(F_{\mu\nu})^2 + \overline{\psi}(i\partial\!\!\!/ - m)\psi - eA_\mu\overline{\psi}\gamma^\mu\psi. \tag{2.1}$$

2. Based on $\mathcal{L}$, we draw all Feynman diagrams that contribute to the process at the desired order. For $e^+e^- \to 2\gamma$ at NLO we have one-loop diagrams multiplying tree-level diagrams (called *virtual corrections*) and tree-level diagrams with an additional photon in the final state, multiplying again such diagrams (called *real corrections*). Often, we will end up with so many diagrams that we would like to have a program generate them for us. Our choice for automatic diagram generation is QGraf [15], a Fortran program capable of generating Feynman diagrams purely based on graph-theoretical concepts. All it needs to know is the kind of lines and vertices at its disposal.

3. We apply the Feynman rules to obtain analytic expressions for amplitudes $\mathcal{A}$ and matrix elements[1] $\mathcal{M} = \mathcal{A}\,\mathcal{A}^\dagger$ in Mathematica. Here $\mathcal{M}_n^{(l)}$ and $\mathcal{A}_n^{(l)}$ have l loops and two photons, $\mathcal{M}_{n+1}^{(l)}$ and $\mathcal{A}_{n+1}^{(l)}$ contain an additional photon in the final state, and so on. Generally, if possible, we reduce the workload, for example by writing the virtual corrections as

$$\mathcal{M}_n^{(1)} = \mathcal{A}_n^{(1)}\,\mathcal{A}_n^{(0)\dagger} + \mathcal{A}_n^{(0)}\,\mathcal{A}_n^{(1)\dagger} = 2Re(\mathcal{A}_n^{(1)}\mathcal{A}_n^{(0)\dagger}), \tag{2.2}$$

   and by computing amplitudes that differ only by permutations of final state momenta just once. In our case we use a custom Mathematica interface of QGraf, which automatically applies the Feynman rules. It can be found at `https://gitlab.com/mule-tools/QGraf`. The version at `https://gitlab.com/mule-tools/QGraf/-/tree/cosmetics` implements the QED Feynman rules given in Section 2.1.

4. Whenever possible, we compute the loop integrals analytically. To that end, we select a regularization scheme, in our case a variant of dimensional regularization, and expand the loop integrals in $d = 4 - 2\epsilon$ dimensions as a Laurent series in ϵ. For evaluation of one-loop integrals, we use the Mathematica program *Package*-X [16] for expansions up to $\mathcal{O}(\epsilon^0)$.

5. We account for contributions with fermion loops, where the quark loops cannot be integrated analytically, since they are non-perturbative at low energies. The method employed here for these contributions is the hyperspherical method, briefly explained in Section 2.4.

6. We express the matrix elements in terms of renormalized quantities. As a result, matrix elements and amplitudes will be free of ultra violet (UV) divergences. We will look at a practical way to do that in Section 2.1.

[1] Note that in contrast to standard convention, the matrix element $\mathcal{M}$ is the product of an amplitude with a complex conjugate amplitude. We call it just the "matrix element", instead of the "matrix element squared".

7. We combine real and virtual corrections to cancel infrared (IR) divergences. In a real-world setting the phase space integrals giving rise to soft divergences cannot be performed analytically. This step therefore requires the introduction of a counterterm that contains the divergence but can be integrated analytically. A systematic way to do this is the FKS^l subtraction scheme [17], whose main ideas are outlined in Section 2.5.

8. We compute an observable cross section by integrating numerically over the final state momenta. Most of the steps above are typically performed in a computer algebra setting; for this step however, we switch to the fast numerical language Fortran 95. Many aspects around the numerical integration have been implemented as part of McMule [18], a Fortran 95 framework for fully differential higher-order QED calculations, on which we rely heavily in this work. In McMule we specify the measurement function, which imposes phase space cuts necessary to match predictions to experiments. For the phase space integration, McMule uses Monte-Carlo (MC) integration in combination with the adaptive importance sampling routine VEGAS [19].

2.1 Diagrammatic renormalization and multiplicative renormalization

Often, renormalization is developed as follows: First, one realizes that the Lagrangian (2.1) actually contains bare quantities that are indicated with 0 subscripts

$$\mathcal{L} = -\frac{1}{4}(F^0_{\mu\nu})^2 + \overline{\psi_0}(i\partial\!\!\!/ - m_0)\psi_0 - e_0 A^0_\mu \overline{\psi_0}\gamma^\mu\psi_0. \tag{2.3}$$

Next, one expresses the bare quantities in terms of renormalized quantities

$$\psi_0 = Z_2^{1/2}\psi, \quad A^\mu_0 = Z_3^{1/2}A^\mu, \quad e_0 = Z_e e, \quad m_0 = Z_m m, \quad e_0 Z_2 Z_3^{1/2} = Z_1 e \tag{2.4}$$

and writes $Z_i = 1 + \delta_i$ so that

$$\begin{aligned}\mathcal{L} &= -\frac{1}{4}Z_3(F_{\mu\nu})^2 + Z_2\overline{\psi}(i\partial\!\!\!/ - Z_m m)\psi - Z_1 e A_\mu\overline{\psi}\gamma^\mu\psi \\ &= -\frac{1}{4}(F_{\mu\nu})^2 + \overline{\psi}(i\partial\!\!\!/ - m)\psi - eA_\mu\overline{\psi}\gamma^\mu\psi \;-\; \frac{1}{4}\delta_3(F_{\mu\nu})^2 + \overline{\psi}(\delta_2 i\partial\!\!\!/ - m(\delta_2 - \delta_m))\psi - e\delta_1\overline{\psi}A\!\!\!/\psi.\end{aligned} \tag{2.5}$$

where we have dropped terms $\mathcal{O}(\delta^2)$ since for simplicity we look at at 1-loop renormalization. The first three terms in (2.5) produce the ordinary Feynman rules

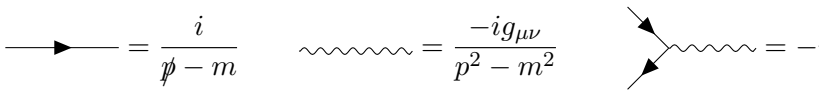

(2.6)

in addition to which we can now read off the counterterms

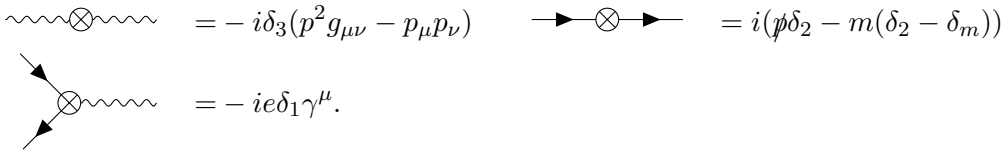

(2.7)

These counterterms allow us to cancel UV divergences in individual diagrams, rendering each diagram by itself finite. That can be useful. For example, the renormalized fermion self-energy $\Sigma(p\!\!\!/)$ in terms of the bare self-energy $\Sigma_0(p\!\!\!/)$ is

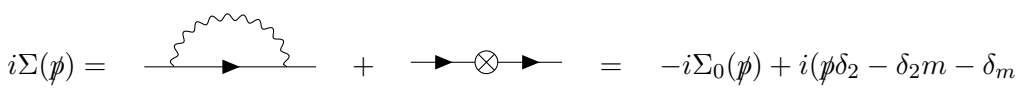

(2.8)

The explicit expressions for δ_2 and δ_m in on-shell renormalization are given in Appendix A for a number of scenarios relevant to this work.
An alternative approach, sometimes called *multiplicative renormalization*, involves less counterterms but does not work for individual diagrams. Instead, the approach renders the full 1-loop amplitude UV finite through application of the following steps:

1. We take the full LO amplitude
2. For each external fermion, we multiply it by a factor of $\sqrt{Z}$ where $Z = Z_1 = Z_2$ due to the Ward identity
3. For each internal fermion line, we send $m \to m + m\delta_m$ to account for mass renormalization
4. We rewrite all factors Z_3^{-1} from internal photons as $Z_3^{-1} = Z_e^2$ and absorb the two charge renormalizations Z_e into the charges of the vertices the photon connects to

Aside from the mass renormalization, which doubles the amount of diagrams, most of the renormalization is thus achieved in a multiplicative way, thus the name multiplicative renormalization. One way to see that multiplicative renormalization is correct is to write $\mathcal{L}$ in the suggestive form

$$\mathcal{L} = -\frac{1}{4} Z_3 (F_{\mu\nu})^2 + Z_2 \overline{\psi}(i\partial\!\!\!/ - m)\psi - Z_2 \overline{\psi}\delta_m \psi - Z_1 e A_\mu \overline{\psi}\gamma^\mu \psi \tag{2.9}$$

which allows us to read off a different set of Feynman rules

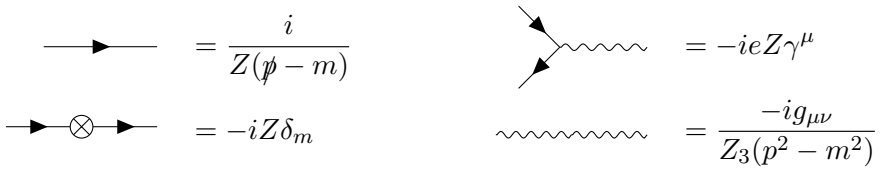

(2.10)

which are similar to (2.6) but contain the Z and Z_3 factors. Now we can write down diagrams using these rules and count the amount of Z factors. For $e^+e^- \to 2\gamma$ we have

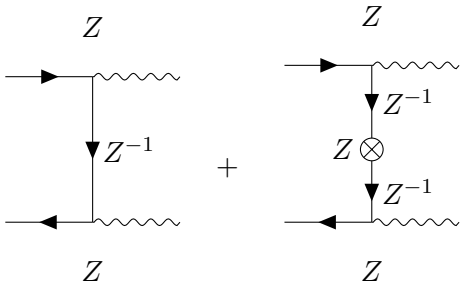

+ *diagrams with loops* (2.11)

where we have written explicitly the different factors of Z. The crux is now to reduce them as much as possible to the ordinary rules (2.6) and some extra bits. The extra bits turn out to be just the mass renormalization, as well as the overall Z factors. To see this, take the first diagram of (2.11). It has a factor Z^{-1} from the propagator and a Z from each vertex, one of which we cancel. Similarly, the second diagram contains after cancellation just an overall factor of Z. Thus (2.11) becomes

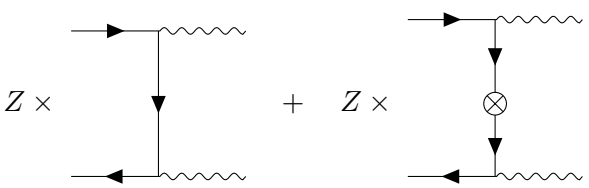

+ *diagrams with loops* (2.12)

which produces the counterterms of the complete NLO amplitude 1-loop amplitude. The nice thing about multiplicative renormalization is that the NLO counterterms can be generated from the tree-level amplitudes, just by splitting up the internal fermion lines and putting in the factors of Z. The definitions of the renormalization constants is equivalent, and they are the same in the two approaches. Having presented the starting point on how one can approach multiplicative renormalization, we would like to refer to chapter 2.1 of [20] for more tips on its practical application.

2.2 LO and NLO conbributions to $e^+e^- \to 2\gamma$

For our process of interest, at leading order we find the tree-level amplitudes

$i\mathcal{A}_n^{(0)} =$ 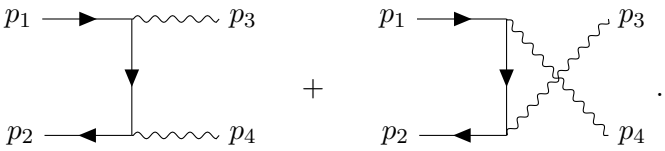

. (2.13)

In terms of the Mandelstam invariants

$$\begin{aligned} s =& (p_1 + p_2)^2 \\ t =& (p_1 - p_3)^2 \\ u =& (p_1 - p_4)^2 \end{aligned} \tag{2.14}$$

the Born matrix element for unpolarized scattering is

$$\mathcal{M}_n^{(0)} = |\mathcal{A}_n^{(0)}|^2 = \quad 32\pi^2\alpha^2 \frac{\left(-m^2\left(s^2+st+t^2\right)+m^4(3s-t)+m^6+t(s+t)^2\right)}{\left(m^2-t\right)^2\left(m^2-s-t\right)} \; + \; (t \leftrightarrow u) \tag{2.15}$$

where m is the electron mass and $\alpha = e^2/4\pi$ the fine structure constant.
Being proportional to $e^4 \sim \alpha^2$, the matrix element (2.15) is the leading order contribution. In general, NLO corrections to our process are $\mathcal{O}(\alpha^3)$ and NNLO corrections will be $\mathcal{O}(\alpha^4)$. The virtual corrections at NLO are produced from tree-level diagrams multiplying the 1-loop diagrams

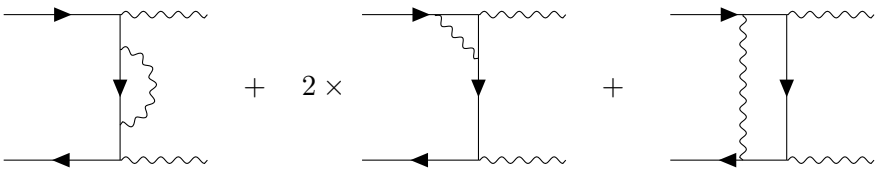

(2.16)

denoted *bubble*, *vertex* and *box* contributions respectively. The diagrams where the final state photons are permuted are always there too, but we will leave them implicit from now on. The factor 2 in (2.16) accounts for the additional diagram with the vertex correction appearing in the lower vertex.
Notice that in (2.16) no diagram contains an internal fermion loop. We call such contributions *photonic*. In addition to (2.16), there are also diagrams with internal fermion loops, which are treated separately in Section 2.4.
The diagrams (2.16) contain UV divergences, and to make them disappear we include the counterterms (2.12). They also contain IR divergences, and to make them disappear we need to account for real corrections, which have an additional photon in the final state. In our process,

real corrections consist of contributions like

$$\mathcal{M}_{n+1}^{(0)} = |\mathcal{A}_{n+1}^{(0)}|^2 = \quad \times \quad + \quad ... \tag{2.17}$$

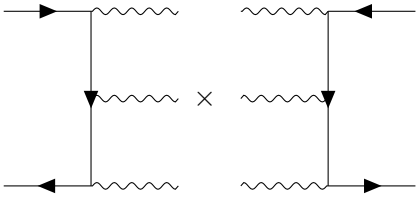

Physically, these diagrams need to be taken into account because if one photon becomes soft (meaning its energy becomes very small), the final state cannot be distinguished from one with just two photons with any realistic detector. There is always a minimum energy that can be detected.
Beyond LO, we do not list any matrix elements directly in this work, since they are lengthy. Instead, we provide all major analytic results in computer readable format [21].

2.3 NNLO contributions to $e^+e^- \to 2\gamma$

At NNLO, we can distinguish three types of contributions: The double-virtual $\mathcal{M}_n^{(2)}$, the real-virtual $\mathcal{M}_{n+1}^{(1)}$ and the double-real $\mathcal{M}_{n+2}^{(0)}$ contributions. Each was obtained in a different manner, and in this section we discuss how.

2.3.1 Double-virtual contributions

First, let us discuss how contributions with two loops were taken into account in this work. The procedure outlined in the following again deals only with the photonic parts (those without fermion loops) and explains how the double-virtual matrix element $\mathcal{M}_n^{(2)}$ with leading mass dependence was obtained. The parts containg fermion loops are discussed in Section 2.4.
We can distinguish two types of double-virtual contributions. On the one hand, we have 1-loop amplitudes multiplying 1-loop amplitudes

$$\mathcal{A}_n^{(1)}\,\mathcal{A}_n^{(1)\dagger} \quad = \quad \times \quad + \quad ... \tag{2.18}$$

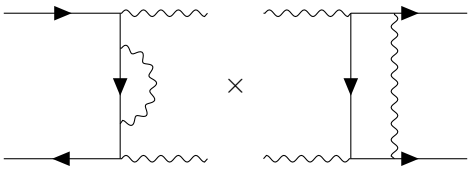

and the other hand, there are two-loop amplitudes multiplying tree-level amplitude

$$\mathcal{A}_n^{(2)}\,\mathcal{A}_n^{(0)\dagger} \quad = \quad \times \quad + \quad ... \tag{2.19}$$

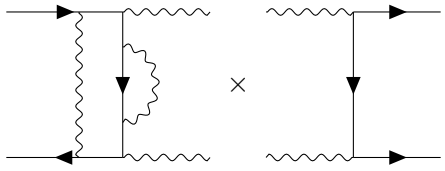

that need to be taken into account.

2.3.1.1 Massification procedure

The two-loop integrals are challenging objects, especially when one would like to obtain the full mass dependence since the integrals can be difficult. Often however, it is enough to construct only the terms that are constant or logarithmic in the fermion mass m while dropping polynomially suppressed terms. This means that terms constant in the fermion mass and terms of order

$\mathcal{O}(\log(m^2/q^2)^n)$ are kept while terms $\mathcal{O}(m^2/q^2)^n$ are not taken into account. Here, q^2 represents an invariant of the process which is much larger than m so the ratio is small (as is the case for the DAΦNE beam where the PADME experiment takes place, which has $\sqrt{s} \approx 1\text{GeV}$).
A procedure dubbed *massification* [22, 23] allows us to obtain this leading mass dependence from the massless variant. The basic principle behind the massification procedure resides in Soft-Collinear Effective Theory (SCET) [24–26]: It can be shown there that the massive variant of the matrix element $M(m)$ can be written in the factorized form

$$\mathcal{M}(m \neq 0) = S \times Z \times \mathcal{M}(0) + \mathcal{O}(m^2/q^2) \tag{2.20}$$

with the soft function S, the process-independet collinear function Z and matrix element with vanishing fermion mass $M(0)$. The soft function S has only contributions from diagrams with fermion loops. It can be shown that all the loop integrals that contain a photon as part of the loop are scaleless in the soft region, and thus vanish in dimensional regularization, a result that has been proven [27] to all orders in perturbation theory within the SCET framework. Since the matrix element $\mathcal{M}$ treated in this section contains no fermion loops, we can set $S = 1$ here. The massification approach has recently been extended beyond NNLO [28,29] and to cases with multiple masses [30].

2.3.1.2 Checking the massless matrix element

The massless variant $\mathcal{M}(0)$ has already been worked out at NNLO [31] a while ago. In this work, the result of [31] was used and massified, thus providing an important shortcut for a difficult part of the NNLO calculation. In order to check the massless results the $\mathcal{A}_n^{(1)}\,\mathcal{A}_n^{(1)^\dagger}$ part was computed independently in this work. Since the ampltiude $\mathcal{A}_n^{(1)}$ is massless, it has pole structure

$$\mathcal{A}_n^{(1)} = \frac{A}{\epsilon^2} + \frac{B}{\epsilon} + C + D\epsilon + ... \tag{2.21}$$

with the ϵ^{-2} pole coming from the overlap of the soft and collinear divergences. In the product $\mathcal{A}_n^{(1)}\,\mathcal{A}_n^{(1)^\dagger}$ all poles up to ϵ^0 need to be retained, and therefore in $\mathcal{A}_n^{(1)}$ all terms up to and including ϵ^2 are needed (since the overlap of the ϵ^2 term and the ϵ^{-2} term is proportional to ϵ^0). Package-X, the Mathematica package for automated ϵ-expansion of one-loop integrals, which was used for all the integrals so far, produces only terms up to ϵ^0.
A separate calculation is therfore required in order to obtain all the photonic 1-loop integrals up to ϵ^2. In a first step, Passarino-Veltman [32] is applied, which is a general method which allows to write tensor integrals in terms of a handful of scalar integrals, thus reducing the amount of integrals that needed to be solved. One then obtains *bubbles* (with two propgators in the loop integral), *triangles* (three propagators in the loop) and *box* integrals, which have four propagators in the loop.
A pedagogical introduction to the methods used for the computation of these integrals is given in [33]. Briefly explained, it proceeds as follows: After conversion of the integrals to parametric Feynman representation, the *bubble* and *triangle* integrals can be rewritten so that the loop integral takes the form of a β function from complex analysis, which in turn is expressed with Γ functions using the identity

$$\int_0^1 dx\; x^{a-1}(1-x)^{b-1} = \beta(a,b) = \frac{\Gamma(a)\Gamma(b)}{\Gamma(a+b)}, \tag{2.22}$$

which yields results exact in ϵ. For the *box* integral, the result exact in ϵ can be found readily using the integral substitution mentioned in [34]. When one applies the substitution, the box

can be written in terms of hypergeometric functions. These can in turn be expanded with the code HypExp 2 [35]. For all integrals, the poles up to and including ϵ^0 were successfully checked against automated calculations. After replacing the integrals, the $\mathcal{A}_n^{(1)}\,\mathcal{A}_n^{(1)\dagger}$ part was obtained up to ϵ^0 and agreement with the result from [31] was found.

2.3.1.3 Conversion to FDH scheme

Since the massification procedure is largely process independent, it is part of the McMule framework and done directly in Fortran. The code though expects the matrix element in the four-dimensional helicity (FDH) scheme, which treats as many objects as possible in strictly four dimensions. The works [18, 36] provide helpful pedagogical introductions to the different regularization schemes.
Application of the procedure therefore requires conversion of the double-virtual matrix element in conventional dimensional regularization (CDR) to the FDH scheme. The key observation that can be exploited for the conversion is the scheme independence of the IR finite matrix element

$$\frac{1}{Z_{\text{CDR}}^2}\left(\mathcal{M}_{\text{CDR}}^{(0)}+\mathcal{M}_{\text{CDR}}^{(1)}+\mathcal{M}_{\text{CDR}}^{(2)}\right) = \frac{1}{Z_{\text{FDH}}^2}\left(\mathcal{M}_{\text{FDH}}^{(0)}+\mathcal{M}_{\text{FDH}}^{(1)}+\mathcal{M}_{\text{FDH}}^{(2)}\right) \tag{2.23}$$

where Z is constructed so that the products in (2.23) are finite for $\epsilon \to 0$. Z has been worked out in dimenional regularization in the massless case [37–40]. In [18] Z is given in FDH, and conversion to CDR is obtained via $n_\epsilon \to 0$. Thus all objects on the left-hand side of (2.23) are now available. On the right-hand side, we can use

$$\mathcal{M}_{\text{FDH}}^{(0)} = \lim_{\epsilon\to 0}\mathcal{M}_{\text{CDR}}^{(0)} \tag{2.24}$$

therefore the only ingredient still required for the prediction of $\mathcal{M}_{\text{FDH}}^{(2)}$ is $\mathcal{M}_{\text{FDH}}^{(1)}$. For this, a full one-loop calculation in FDH is required. In this scheme regular fields are treated in 4 dimensions while singular fields are treated in $d_s = d + n_\epsilon$ dimensions ($d = 4 - 2\epsilon$). As a result, when going from CDR to FDH the diagrams with ϵ-scalars can be generated from

$$g_{[d]}^{\mu\nu} \to g_{[d]}^{\mu\nu} + \frac{e_e^2}{e^2} g_{[n_\epsilon]}^{\mu\nu} \tag{2.25}$$

where in brackets we denote the dimension of the space the objects live in. Pictorially,

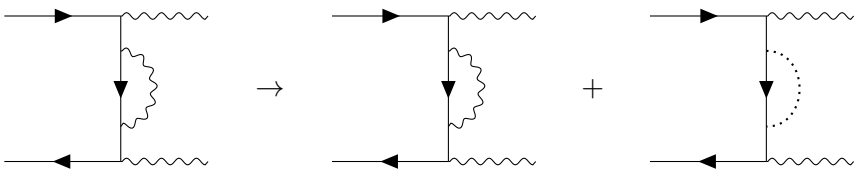

(2.26)

where the second diagram in (2.26) has an ϵ-scalar in the loop. When evaluating the diagrams, we need the ability to deal with the numerator algebra mandated from the hierarchy

$$S_{[4]} \subset QS_{[d]} \subset QS_{[d_s]} \tag{2.27}$$

of the spaces involved, using the same notation as [18]. To aid in this calculation, we use the Mathematica package TRACER [41], which can do algebra with Dirac γ matrices in arbitrary dimensions.

2.3.2 Real-virtual contributions

Real-virtual contributions consist of one-loop diagrams with an additional photon in the final state multiplying tree-level diagrams with an additional photon, e.g.

$\mathcal{M}^{(1)}_{n+1} =$ 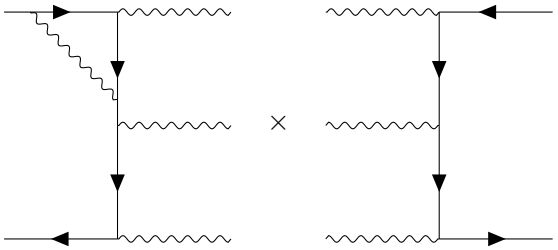 $+ \quad ...$ (2.28)

Instead of calculating $\mathcal{M}^{(1)}_{n+1}$ by ourselves we decided to use OpenLoops 2 [42–44], a Fortran program that allows to evaluate tree and one-loop scattering matrix elements for any SM process automatically.
In order to see if OpenLoops was indeed viable even in the limit where one of the photons is soft, its numerical stability was studied for decreasing photon energy in an otherwise random phase space point. To study the energy decrease we introduce the dimensionless scaled photon energy ξ defined via

$$E_\gamma = \frac{\sqrt{s}}{2}\xi \tag{2.29}$$

with photon Energy E_γ, and compare real-virtual matrix element to the eikonal approximation, which is defined in Section 2.5. The results, shown in Figure 2.1 in terms of ξ, suggest that

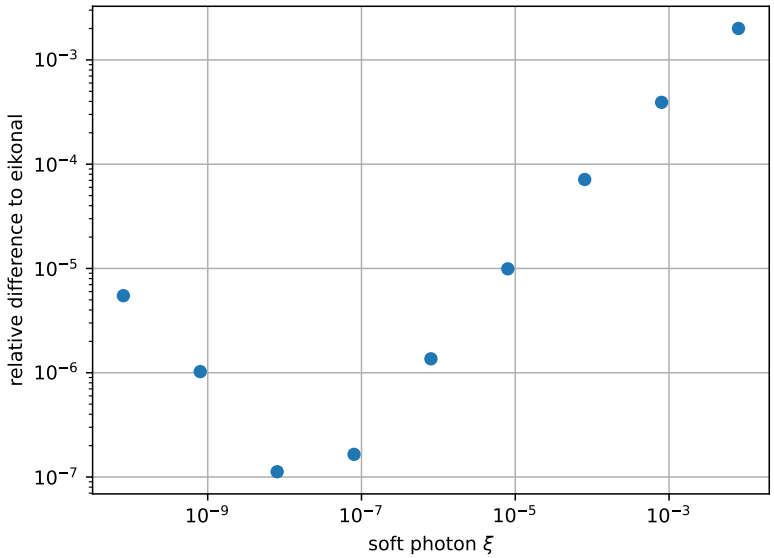

Figure 2.1: Relative agreement of $\mathcal{M}^{(1)}_{n+1}$ to the eikonal approximation, evaluated with OpenLoops 2 for decreasing photon energies parameterized by ξ.

as we decrease the soft photon energy the agreement with the eikonal approximation increases. Only when we reach $\xi \approx 10^{-8}$ the agreement starts to become worse, a behavior which can most likely be attributed to numerical instabilities which arise at this point. But even at $\xi \approx 10^{-10}$ the relative agreement is still $\mathcal{O}(10^{-5})$. In the soft-collinear region it was also found that the

numerical stability is fine. Therefore we decided to use OpenLoops 2 in this work for the evaluation of $\mathcal{M}^{(1)}_{n+1}$.

2.3.3 Double-real contributions

We also need to account for double-real contributions. They are products of tree-level amplitudes with four photons in the final state, that is

$\mathcal{M}^{(0)}_{n+2} =$ 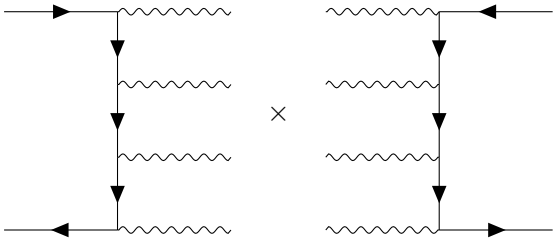 $+ \quad ...$ (2.30)

The double-real contributions are arguably the simplest NNLO pieces. Aside from the different permutations of the final state photons, the topology shown in (2.30) is the only one that needs to be taken into account. While $\mathcal{M}^{(0)}_{n+2}$ can be evaluated with OpenLoops 2, it was decided to obtain an analytical expression for the matrix element by ourselves, since it is faster than OpenLoops 2 and a lot of statistics for the double-real contribution is needed.
Thus $\mathcal{M}^{(0)}_{n+2}$ was calculated in Mathematica, and the result agrees with OpenLoops 2. The long fermion line produces a multitude of terms when one performs the spin sum. In addition, from final state permutations there are $4! = 24$ individual diagrams that produce 24×24 contributions[2] to $\mathcal{M}^{(0)}_{n+2}$. Naive calculation of $\mathcal{M}^{(0)}_{n+2}$ produces numerical instabilities. Fortunately, these seem to go away when one simplifies separately chunks of 24 diagrams (all permutations) multiplying one single diagram. An overall simplifcation was not done.

2.4 Contributions with fermion loops

Contributions with internal fermion loops, also called n_F contributions, can be divided into vacuuum polarization (VP) contributions that contain insertions of

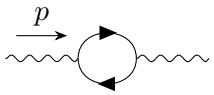 $= ip^2 g_{\mu\nu}\Pi(p^2)$ (2.31)

and light-by-light (LbL) contributions that have insertions of

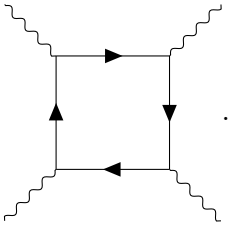 . (2.32)

Fermion loops with an odd number of photons attached vanish as a result of Furry's theorem [14]. At NLO, in our process of interest there is only one fermion loop contribution, namely

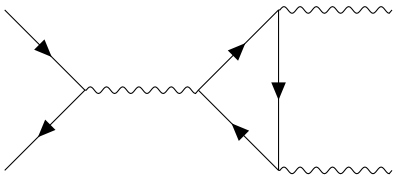 $= 0$ (2.33)

[2]From these, only $24 \times 25/2 = 300$ are unique, corresponding to the upper triangle of the 24×24 matrix

which is zero (it has three photons attached to the loop). Therefore there are no fermion loop contributions to $e^+e^- \to 2\gamma$ at NLO.
In general, the loop fermion can be any lepton or quark, with each possibility giving another diagram. At low energies, the analytical form of hadronic contributions (those with quark loops) is unknown. Accounting for such contributions presents a major challenge since they cannot be obtained in perturbative QCD.
Let us first look at VP contributions. These arise from insertion of (2.31) into internal photons. The action of the insertion into a photon propagator is

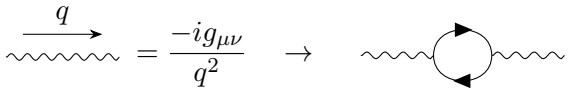

$$= \frac{-ig_{\mu\nu}}{q^2} \quad \to \quad = \frac{-ig_{\mu\alpha}}{q^2} iq^2 g_{\alpha\beta}\Pi(q^2)\frac{-ig_{\beta\nu}}{q^2} = \frac{-ig_{\mu\nu}}{q^2}\Pi(q^2) \tag{2.34}$$

and thus corresponds to just a multiplication with $\Pi(q^2)$. Since in our process of interest there are no internal photons at LO, VP diagrams arise from the insertion into NLO diagrams and therefore contribute only at NNLO. Therefore we have *bubble*, *vertex* and *box* contributions at NNLO given by the corresponding one-loop contribution multiplied by $\Pi(q^2)$, where q^2 is the loop momentum.
To account for these contributions there exist two strategies: The hyperspherical method, which has been historically used to evaluate the QED parts of the electron $g-2$ [45–47], and the dispersive method [48, 49]. In this work we proceeded with the hyphersperical method, which is pedagogically introduced in [50]. Very briefly, the method works like this:

1. Fix the momentum routing such that the momentum flowing through the VP is q^2, so that one has $\Pi(q^2)$.

2. Wick rotate the loop and external momenta into the Euclidean momenta (denoted by capital letters) and write the loop momentum in terms of hyperspherical coordinates, which gives the Jacobian
$$d^4q = id^4Q = i\frac{Q^2}{2}dQ^2 d\Omega_Q \tag{2.35}$$

3. Reduce to a set of master integrals, which can be achieved with Passarino-Veltman reduction [32]. However, we may not use the implementation `PVReduce` [51] (which is part of Package-`X`), since it uses properties that we are not allowed to use in the present case; namely shift invariance and the fact that scaleless integrals vanish in dimensional regularization[3]. Thus a custom version of the algorithm by Passarino and Veltman was implemented to perform the reduction to scalar integrals.

4. Integrate over the angles $d\Omega_Q$, leaving only a residual radial dQ^2 integration.

5. Rotate all momenta back to Minkowski space and perform the analytical continuation.

Looking at the structure of the angular integrals arising in our calculation it can be observed that the bubble contribution contains integrals with only a single angle-dependent propagator. The vertex and box contributions contain integrals with maximum two and three angle-dependent propagators respectively. Therefore all angular integrals can be reduced to three scalar master

[3] We cannot use shift invariance since we still have a factor of $\Pi(q^2)$ in every term. Shifting the loop momentum therefore results in a different value of $\Pi(q^2)$. Moreover, integrals that would otherwise be scaleless are not due to $\Pi(q^2)$.

integrals, which can be computed in the hyperspherical method. The first two are

$$\begin{aligned}\int d\Omega_Q \; \frac{1}{(Q+P_1)^2+m_1^2} &= 2\pi^2 \, \frac{\mathcal{Z}_1}{\sqrt{Q^2 P_1^2}} \\ \int d\Omega_Q \; \frac{1}{(Q+P_1)^2+m_1^2} \, \frac{1}{(Q+P_2)^2+m_2^2} &= \frac{i\pi^2}{Q^2\sqrt{P_1^2 P_2^2(1-\tau)}} \; \log\left(\frac{1+z\tau+iz\sqrt{1-\tau^2}}{1+z\tau-iz\sqrt{1-\tau^2}}\right)\end{aligned} \tag{2.36}$$

where we have introduced the abbreviations

$$\begin{aligned}\mathcal{Z}_i &= \frac{Q^2+P_i^2+m_i^2-\sqrt{\lambda(Q^2,P_i^2,-m_i^2)}}{2\sqrt{Q^2P^2}} \qquad \text{for } \; i=1,2 \\ z &= \; -\mathcal{Z}_1\mathcal{Z}_2 \\ \tau &= \frac{P_1\cdot P_2}{\sqrt{P_1^2P_2^2}}.\end{aligned} \tag{2.37}$$

Here $\lambda(a,b,c)$ is the Källén function and all dot products and squares of four-dimensional objects are defined in terms of the four-dimensional Euclidean metric. The integrals (2.36) were obtained through expansion of the angle-dependent propagators in terms of Gegenbauer polynomials and through application of orthogonality relations of the Gegenbauer polynomials. The product of three angle-dependent propagators, which we require for the box contribution, cannot be obtained in this way since the integral of a product of three Gegenbauer polynomials is not known. The master integral with three angle-dependent propagators was taken from [52], where it has been computed by direct integration.

At this point, the residual Q^2 integrals still contain UV divergences. Again, these can be removed by including the counterterms (2.12), but now the counterterms are computed in the hyperspherical method, too. The fermion self-energy at 1-loop is thus integrated over the angles of the loop momentum, for which we can use the master integrals (2.36) again. The resulting Q^2 dependent renormalization constants are given in Appendix A.

Having completed the angular integration, many aspects of the result can be checked by choosing

$$\Pi(q^2) = \frac{q^2}{q^2-\lambda^2} \tag{2.38}$$

then the vacuum polarization becomes

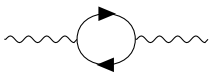

$$= \frac{-ig_{\mu\nu}}{q^2}\Pi(q^2) = \frac{-ig_{\mu\nu}}{q^2-\lambda^2} \tag{2.39}$$

which corresponds to the propagator for a massive photon. With this choice, the integral over q^2 is finite, because the IR divergence has been regulated by the finite photon mass. With this choice of Π, we can thus integrate numerically. At the same time, we can now integrate analytically, since there are just one-loop integrals, although with massive photons. Again, the result needs to be rendered UV finite by including the counterterms, which are computed from the fermion self energy with a massive photon correction. To allow for a precise comparison, the renormalization constants were computed including terms polynomial in λ. The results are also given in Appendix A. The comparison of the numerical and analytical integration was then performed for different phase space points, and the relative agreement between the two turned out to be of the order of 10^{-8} to 10^{-20}.

2.5 Dealing with infrared divergences

Once the real and virtual matrix elements have been obtained, they need to be integrated over the phase space in order to produce an observable cross section. In this section, we discuss how this can be achieved at NLO.
The NLO contribution to the cross section for a process with n final state particles can be written in terms of the virtual and real matrix elements $\mathcal{M}_n^{(1)}$ and $\mathcal{M}_{n+1}^{(0)}$ as

$$\sigma = \int d\sigma_v + \int d\sigma_r = \int d\Phi_n \mathcal{M}_n^{(1)} + \int d\Phi_{n+1} \mathcal{M}_{n+1}^{(0)} \tag{2.40}$$

where $d\Phi_n$ is the n-particle phase space volume

$$d\Phi_n = (2\pi)^4 \delta(\Sigma k) \prod_i d\phi_i = (2\pi)^4 \delta(\Sigma k) \prod_i \frac{d^3\vec{k}_i}{(2\pi)^3 2E(\vec{k}_i)}. \tag{2.41}$$

The issue at this point is that the real and virtual contributions in (2.40) are both separately IR divergent. If we could compute the integrals analytically, then the divergences would manifest in terms of the regulator used, and the dependence on the regulator would drop out once real and virtual contributions are combined, as guaranteed by the KLN theorem [53, 54]. This is indeed possible for simple observables, and it has been accomplished at NLO for $e^+e^- \to 2\gamma$ in [55].
But often we cannot integrate analytically, especially when considering also the presence of the measurement function that imposes non-trivial phase space cuts in order to match experimental procedures. The measurement function along with the flux factor have been left implicit in (2.40). We are thus left with numerical phase space integration as the only option.
The trick is to construct a counterterm $\mathcal{M}_{\text{CT}}$ that contains the divergence and can be integrated analytically. The counterterm can then be subtracted from the real corrections and added back

$$\int d\phi_\gamma \left(\mathcal{M}_{n+1}^{(0)} - \mathcal{M}_{\text{CT}} \right) + \int d\phi_\gamma \, \mathcal{M}_{\text{CT}}. \tag{2.42}$$

Because it can be integrated analytically over the additional photon phase space $d\phi_\gamma$, the integrated counterterm can then be combined with the virtual correction, making it finite as well.
A general method for the construction of such a counterterm, originally proposed by Frixione, Kunszt and Signer [56] and recently generalized to any order in perturbation theory [17] in massive QED, is to isolate the soft part of the real contribution in a delicate way. To start, we parameterize the photon that can become soft with scaled energy ξ, cosine of the angle y and a $(d-2)$-dimensional transversal unit vector $\vec{e_T}$ as

$$k = \frac{\sqrt{s}}{2} \xi (1, \sqrt{1-y^2}\vec{e_T}, y) \tag{2.43}$$

so that in the soft limit $\xi \to 0$. Then the phase space $d\phi_\gamma$ of the extra photon can be split into radial and angular integrals

$$d\phi_\gamma = \mu^{4-d} \frac{d^{d-1}k}{(2\pi)^{d-1} 2E(\vec{k})} = d\Upsilon d\xi \xi^2 \xi^{-1-2\epsilon} \tag{2.44}$$

where Υ includes the angular part and some trivial factors. A ξ^2 has been factored out explicitly in order to apply to the remaining $\xi^{-1-2\epsilon}$ the identity

$$\begin{aligned} \xi^{-1-2\epsilon} &= -\frac{\xi_c^{-2\epsilon}}{2\epsilon} \delta(\xi) + \left(\frac{1}{\xi^{1+2\epsilon}} \right)_c \\ \left\langle \left(\frac{1}{\xi^n} \right)_c, f \right\rangle &= \int_0^1 d\xi \frac{f(\xi) - f(0)\theta(\xi_c - \xi)}{\xi^n}. \end{aligned} \tag{2.45}$$

ξ_c can be fixed arbitrarily as long as it is in the same range as ξ. However, keeping it variable can serve as a check of the implementation of the scheme. In Chapter 3, this ξ_c independence is verified for our process of interest.
When replacing $\xi^{-1-2\epsilon}$ the real corrections become

$$d\sigma_r = d\sigma_s + d\sigma_h = \int d\Upsilon d\phi_{n,1} d\xi \left(-\frac{\xi_c^{-2\epsilon}}{2\epsilon} \delta(\xi) \mathcal{M}_{n+1}^{(0)} \xi^2 + \left(\frac{1}{\xi^{1+2\epsilon}} \right)_c \mathcal{M}_{n+1}^{(0)} \xi^2 \right) \tag{2.46}$$

with $d\phi_{n,1}$ being the phase space of the remaining particles. The first term in (2.46) can be trivially integrated over $d\xi$ due to the presence of $\delta(\xi)$, and the result amounts to evaluating the real matrix element $\mathcal{M}_{n+1}^{(0)}$ in the soft limit, which simplifies to the well-known result

$$\lim_{\xi \to 0} \xi^2 \mathcal{M}_{n+1}^{(0)} = \mathcal{E} \mathcal{M}_n^{(0)} \tag{2.47}$$

with Born matrix element $\mathcal{M}_n^{(0)}$ and process-independent eikonal factor $\mathcal{E}$. In the soft part (the first summand in (2.46)), the only dependence on the extra photon momentum is in $\mathcal{E}$, which can be integrated analytically over the extra photon phase space in dimensional regularization, thus producing the integrated eikonal

$$\hat{\mathcal{E}}(\xi_c) = -\frac{\xi_c^{-2\epsilon}}{2\epsilon} \int d\Upsilon \mathcal{E}. \tag{2.48}$$

The integrated eikonal contains explicit $1/\epsilon$ poles from the soft singularities, which cancel the $1/\epsilon$ poles in the virtual contributions. The real and virtual contributions can then be written as

$$\sigma = \sigma_v(\xi_c) + \sigma_r(\xi_c) = \int d\Phi_n \left(\mathcal{M}_n^{(1)} + \hat{\mathcal{E}}(\xi_c) \mathcal{M}_n^{(0)} \right) + \int d\Phi_{n+1} \left(\frac{1}{\xi} \right)_c (\xi \mathcal{M}_{n+1}^{(0)}), \tag{2.49}$$

the integrands are now separately finite and can thus be comptuted numerically in strictly $d = 4$ dimensions.
At higher orders in perturbation theory the idea remains the same: As long as we have something divergent, we split it up with counterterms until we end up with finite integrands. For the construction of these counterterms, we use the factorization of the all orders matrix element into an exponential involving the eikonal and a finite part [57]

$$\sum_{l=0}^{\infty} \mathcal{M}_n^{(l)} = e^{-\alpha \mathcal{E}} \sum_{l=0}^{\infty} \mathcal{M}_n^{(l)f}. \tag{2.50}$$

The generalization of the infrared subtraction at any order in perturbation theory is discussed in [17] in detail.

2.6 Dealing with numerical instabilities

In the evaluation of the MC integrand, numerical instabilities can arise. For example, in the hyperspherical method, the UV cancellation can be problematic: In the large Q^2 regime the counterterms subtract a large number from a large number, yielding an inaccurate small result. In this section, after discussing how they can arise, we mention some strategies to battle such instabilities.
Evaluating expressions with a large number of digits (e.g. 100) in Mathematica and comparing to evaluation with machine precision can serve as a measure for numerical instability. The underlying reason for the instabilities resides in the finite representation of rational numbers

in computers. Nowadays, floating-point numbers are almost always represented in terms of the IEEE 754 standard, which approximates numbers using their scientific representation:

$$number = (-1)^s \times m \times b^e. \tag{2.51}$$

For example in single precision, base $b = 2$ is used, 1 bit is reserved for the sign (s) of the number, 8 bits for the exponent e and 32 bits for the mantissa m, requiring in total 32 bits.
For the sake of argument, let us imagine that we have a decimal machine ($b = 10$) with a mantissa of just five decimal digits and we would like to subtract 4199.926123 from 4200.00000. Now, when we load these numbers into variables they will be represented as 4.1999×10^3 and 4.2000×10^3 (these are each separately accurate to five digits). The result of the subtraction on the other hand will be 1.0000×10^{-1} which has an accuracy of only a single digit; the true result being 0.073877.
There are several ways to battle these problems:

1. Perform the bulk of the subtraction *before* the conversion to the floating point system.

2. Using identities, rewrite expressions to make the cancellation less extreme. For example, for $|a| \approx |b|$ we replace
$$a^2 - b^2 \quad \rightarrow \quad (a+b)(a-b) \tag{2.52}$$
since $a^2 - b^2$ loses twice as many digits as $(a+b)(a-b)$ does[4]. Another variation of this occurs when we we want to compute $p_0 - |\vec{p}|$ for an on-shell momentum where $|\vec{p}| \gg m$. Then we should always replace
$$p_0 - |\vec{p}| \quad \rightarrow \quad (\, p_0 - |\vec{p}|\,) \frac{p_0 + |\vec{p}|}{p_0 + |\vec{p}|} = \frac{m^2}{p_0 + |\vec{p}|} \tag{2.53}$$
which replaces the problematic *large - large* with a well-behaved *small / large*.

3. In the problematic region, expand the expression in a small parameter. For example, the following logarithm, which arose from the VP contributions, is improved through expansion in the small parameter m^2/s
$$\log\left(\frac{s - \sqrt{s\,(s-4m^2)} - 2m^2}{s + \sqrt{s\,(s-4m^2)} - 2m^2}\right) = 2\log\frac{m^2}{s} + \frac{4m^2}{s} + ... \tag{2.54}$$
where we include as many terms as needed for our target accuracy.

4. Switch to higher precision, e.g. quadruple precision. This makes the evaluation of the expression slower, but depending on where the bottleneck is, it might not matter.

[4]Besides, $a^2 - b^2$ is also slower since it has two multiplications and one addition versus two additions and one multiplication.

3 Results

In this chapter, we present numerical results for Born, NLO and NNLO cross sections. The results include photonic contributions only.

3.1 Integrated cross sections and implementation tests

The calculation of QED corrections in the FKS^l scheme require the introduction of the unphysical parameter ξ_c as introduced in Section 2.5. Therefore, independence of the radiative corrections from ξ_c needs to be checked at NLO and NNLO. This is successfully demonstrated for values in the range of $0.01 \leq \xi_c \leq 1$ with the NNLO results shown in Figure 3.1. A plot demonstrating ξ_c independence at NLO can be found in Appendix B.

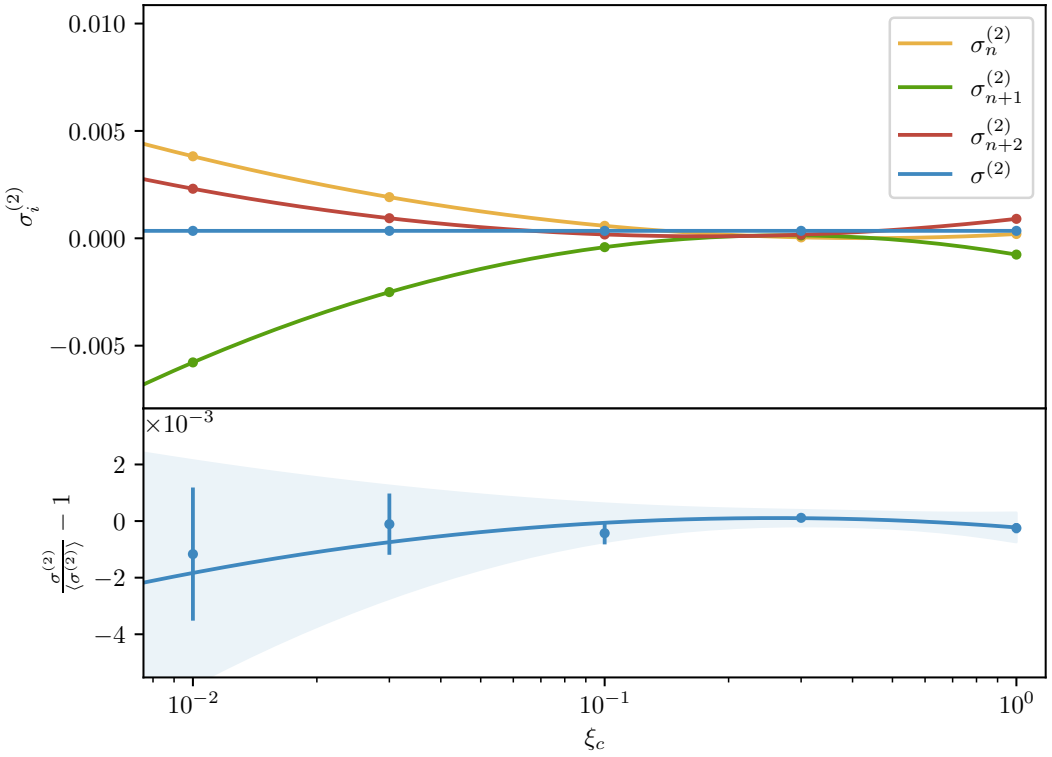

Figure 3.1: Demonstration of ξ_c independence for the integrated cross section $\sigma^{(2)}$. Top: IR finite double-virtual, real-virtual, double-real and combined cross sections as a function of ξ_c. Bottom: Quadratic fit and relative difference of $\sigma^{(2)}$ to fitted cross section with 2σ confidence in shaded blue.

The results were obtained at $\sqrt{s} = 1.0$ GeV for an observable that models the DAΦNE criteria:

We ask for at least two photons in the final state satisfying

$$\begin{aligned} E_{\min} &= 300 \text{ MeV} \\ 45^\circ < \theta &< 135^\circ \\ \xi_{\max} &= 10^\circ \end{aligned} \tag{3.1}$$

where $\xi = |180^\circ - \theta_1 - \theta_2|$ is the acollinearity between the most energetic and next-to-most energetic photon, θ_i the angle of photon i to the beam axis and $E_{\min}$ the minimum photon energy.
The resulting Born, NLO and NNLO corrections along with MC errors are summarized in Table 3.1. We give the LO cross section $\sigma^{(0)}$ as well as the NLO and NNLO corrections $\sigma^{(1)}$ and $\sigma^{(2)}$ from McMule and BABAYAGA event generator, taken from [58], where $\sigma^{(2)}$ is based on an approach that matches the exact NLO result to a parton shower algorithm. In addition, we give the ratio of full cross sections at subsequent orders

$$K^{(i)} = 1 + \delta K^{(i)} = \frac{\sigma_i}{\sigma_{i-1}} \tag{3.2}$$

where σ_i is the full cross section at order i, e.g. $\sigma_2 = \sigma^{(0)} + \sigma^{(1)} + \sigma^{(2)}$.

	σ (nb)	BABAYAGA σ (nb)	McMule $\delta K^{(i)}(\%)$
$\sigma^{(0)}$	137.53087(3)	137.53	
$\sigma^{(1)}$	-8.08773(9)	-8.08	-5.88067
$\sigma^{(2)}$	0.38298(3)	0.32	0.296

Table 3.1: Resulting integrated LO, NLO and NNLO corrections and MC numerical errors for the criteria (3.1) obtained with McMule compared to BABAYAGA.

	σ (nb)	$\delta K^{(i)}(\%)$
$\sigma^{(0)}$	132.19035(2)	
$\sigma^{(1)}$	-0.4472(2)	-0.3383
$\sigma^{(2)}$	0.00405(8)	0.0031

Table 3.2: Resulting corrections for an observable similar to (3.1) but without the cut on acollinearity

At LO and NNLO, we find agreement to BABAYAGA in all digits provided in [58]. At NNLO, our cross section agrees to the matched parton shower at the level of 19%. In Table 3.2 the results for the observable (3.1) but without the acollinearity cut are shown. We note that the NLO cross section is an order of magnitude smaller than the result obtained with the $\xi_{\max}$ criterion, and the NNLO correction is two orders of magnitudes smaller. The sizeable radiative corrections in Table 3.1 are a consequence of the $\xi_{\max}$ cut.

3.2 Differential distributions

Besides the integrated cross sections, a number of differential distributions for the criteria (3.1) were obtained. Figure 3.2 displays the distribution of acollinearity. In Figure 3.3 and Figure 3.4 we show the energy distribution of the most and next-to-most energetic photon in the top panel. In Figures 3.5 and 3.6 the distributions of θ_1 and θ_2 are given, where we only give the NLO results, since the NNLO results require more statistics than have been obtained at the time of

writing. In the top panel of each plot we show the distrubtion over x of the total cross sections $d\sigma/dx$ while in the bottom pannel we display the distribution of the K-factors defined as

$$K^{(i)} = 1 + \delta K^{(i)} = \frac{d\sigma_i/dx}{d\sigma_{i-1}/dx}. \tag{3.3}$$

Let discuss Figure 3.3, the energy distribution of the most energetic photon. It can be observed that the NLO curve vanishes below $E_1 \approx 330$ MeV. This is because the situation where the most energetic photon has the least energy happens when the energy is distributed evenly among the three photons available at NLO, i.e. for $E_i = \sqrt{s}/3 \approx 330$ MeV. By the same reasoning the NNLO curve would drop to zero at $E_1 = \sqrt{s}/4 = 250$ MeV. However, it is zero below $E_1 = 300$ MeV simply due to the criteria (3.1).
As discussed in Section 3.1, one reason for the sizeable corrections observed is the cut on acollinearity. Adding to this, many distributions have the LO cross concentrated in a single bin. As a result, in the bins that have no contribution from the LO, the NNLO correction represents in fact an NLO correction, thus enhancing the K-factors significantly. For example, in Figure 3.4 we have $\delta K^{(2)}$ of the same order of magnitude as $\delta K^{(1)}$ in Figure 3.5.

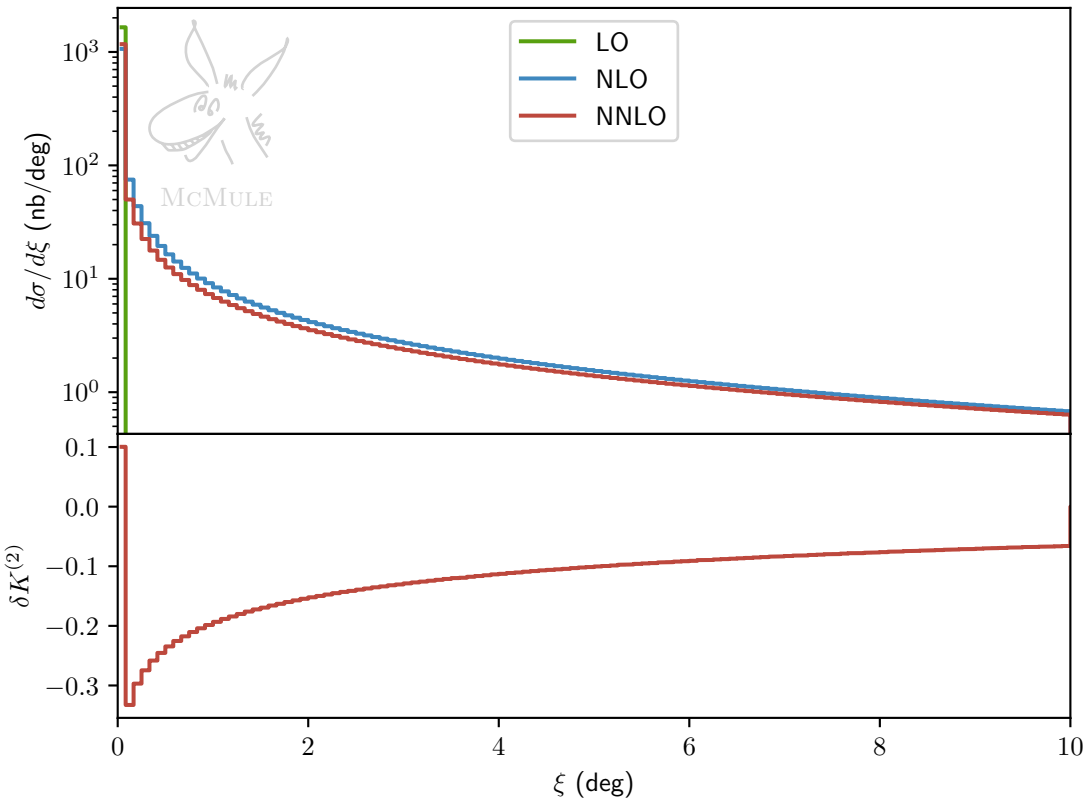

Figure 3.2: Distribution of acollinearity between most energetic and next-to-most energetic photon

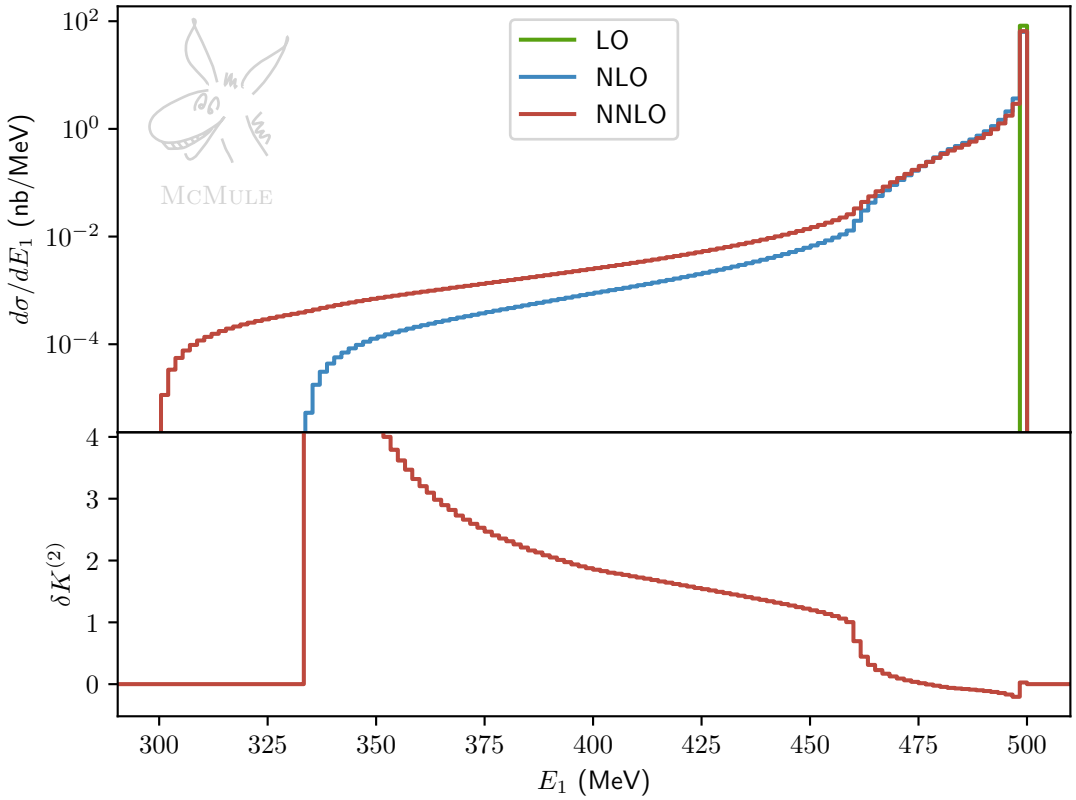

Figure 3.3: Energy distribution of the most energetic photon

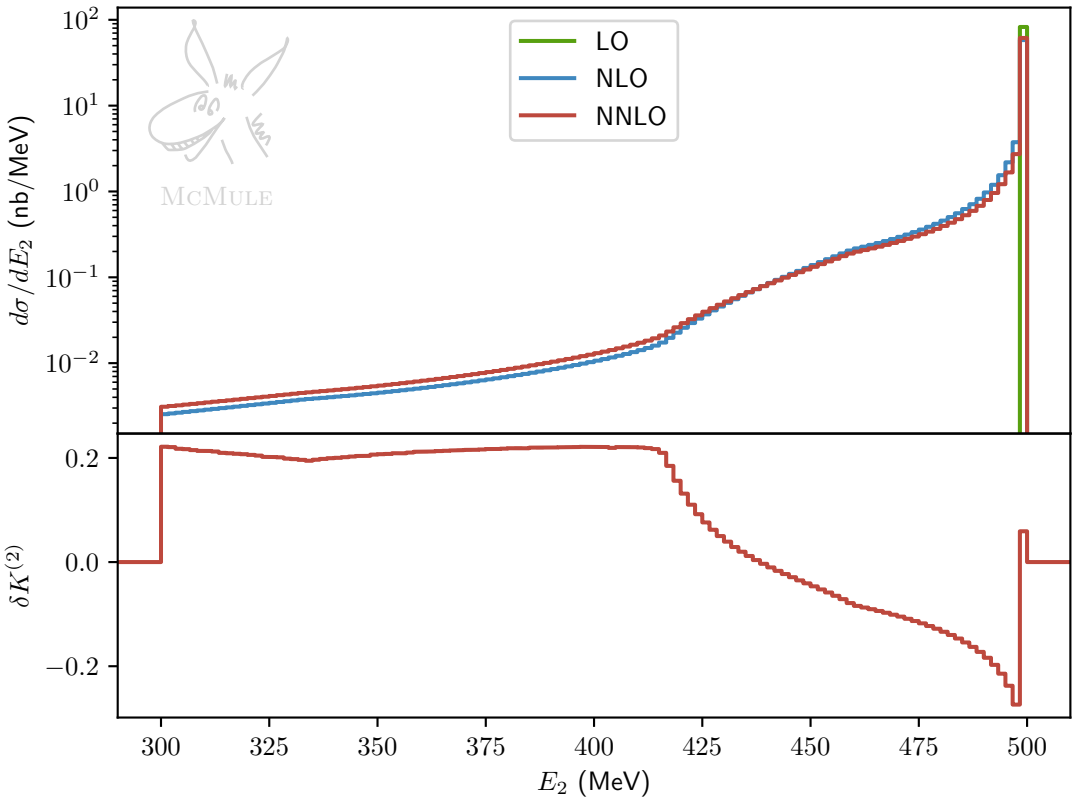

Figure 3.4: Energy distribution of the next-to-most energetic photon

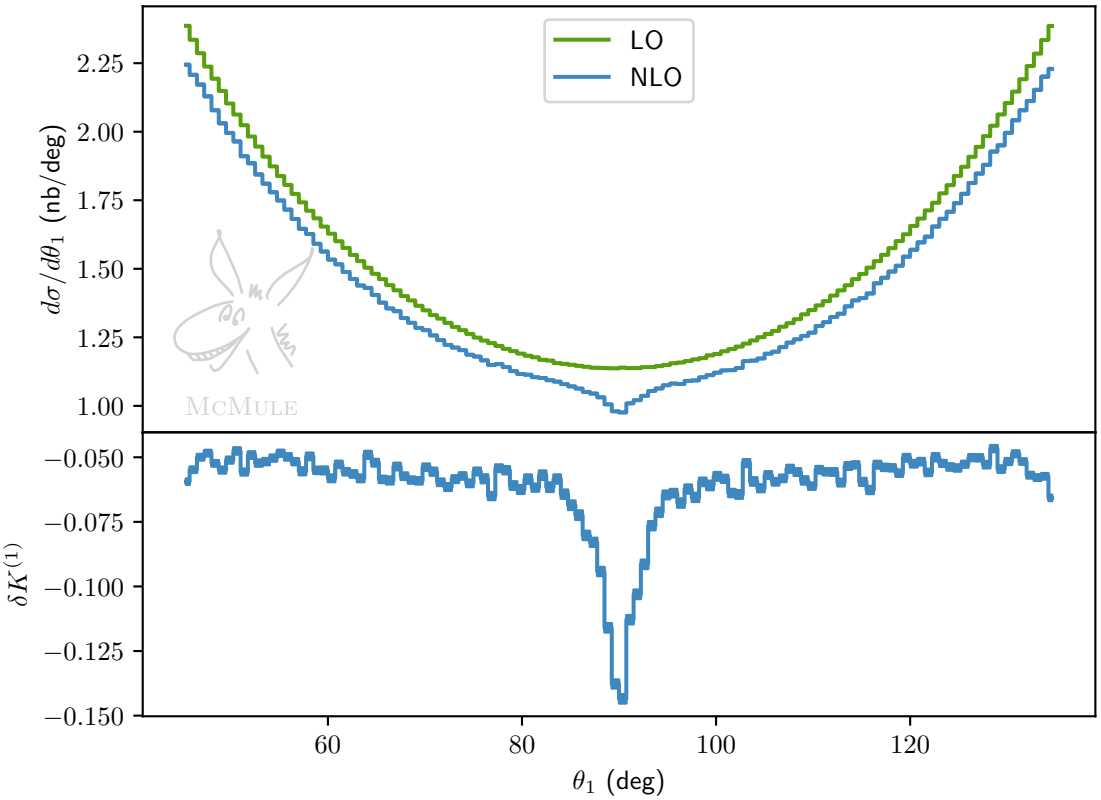

Figure 3.5: Angular distribution of the most energetic photon

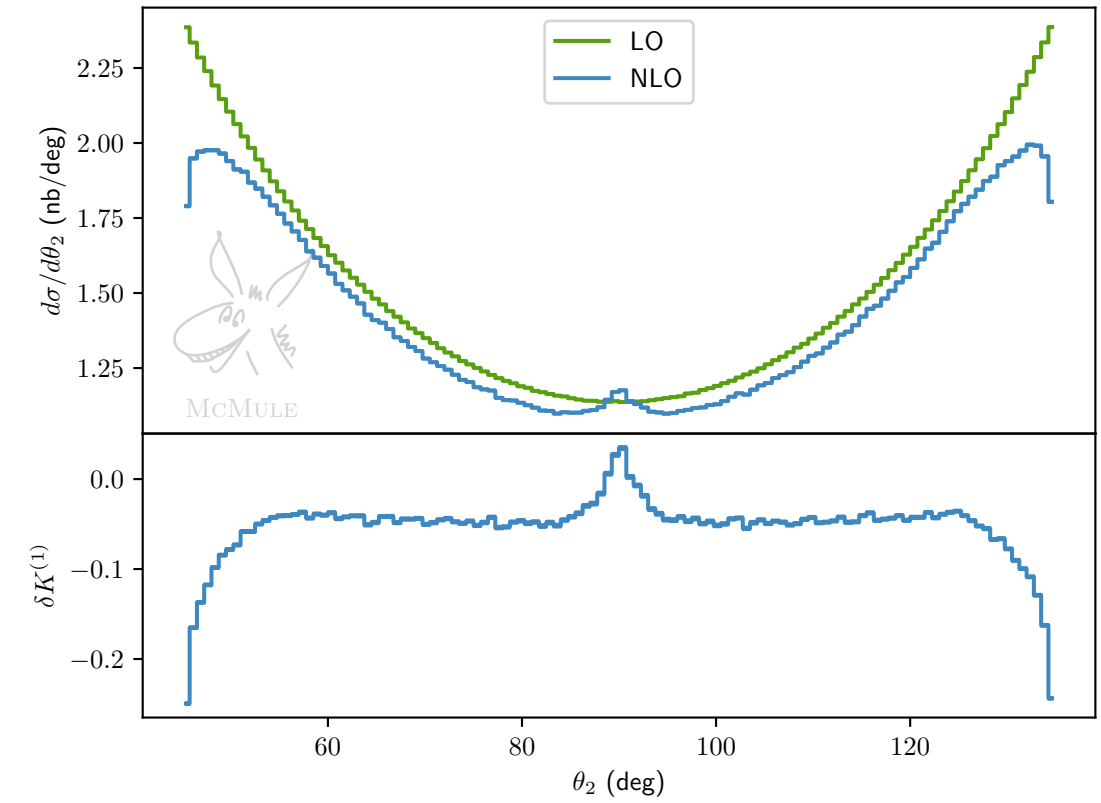

Figure 3.6: Angular distribution of the next-to-most energetic photon

4 Conclusion and outlook

$e^+e^- \to 2\gamma$ is a process of interest in low-energy precision physics, for example in light of the PADME experiment that uses the process to search for BSM signals. In this master thesis, we have performed a high-precision QED calculation for $e^+e^- \to 2\gamma$. For the first time, fixed order NNLO corrections are accounted for in this process, and as a result, we are able to obtain photonic NNLO contributions for any observable. The NNLO correction accounts for effects constant and logarithmic in the electron's non-vanishing mass, while some polynomial terms are neglected. The calculation, which has been cross-checked at LO, NLO and NNLO with BABAYAGA at the level of integrated cross sections, is implemented in the latest version of McMule [18], which is publicly available.

At the time of writing, the calculation accounts for photonic contributions. Leptonic and hadronic VP contributions have been prepared already as part of the thesis, but are not yet included in the numerical results. The natural next step is therefore to include VP contributions. As for the hadronic LbL contributions, one would probably have to switch from the hyperspherical method to a dispersive Ansatz. Essentially, it is expected that a lot of the work done for the hadronic contributions to $g-2$ will have to be redone, of which an overview can be found in [59]. Possibly, one could use a similar parameterization of the hadronic LbL tensor, although the presence of at least two real photons might simplify things.

Finally, the results obtained in the present work may provide a shortcut to the related process $e^-\gamma \to e^-\gamma$ (Compton scattering) through crossing relations. The massless two-loop results that were obtained contain the full complex dependence, thus after crossing the analytic continuation to the physical domain should be feasible.

Increased accuracy for photonic contributions could be obtained through incorporation of a parton shower algorithm. One could also work towards an $\mathrm{N^3LO}$ calculation: The FKS scheme has been generalized to any order in perturbation theory for QED, and massless matrix elements have recently been worked out in [60] and [61]. Although it is expected that the three-loop matrix elements will present a major bottleneck, targeting the next order frontier can become an achievable task in the forseeable future.

Bibliography

[1] R. Oerter, *The theory of almost everything: The standard model, the unsung triumph of modern physics* (2006).

[2] J.D. Lykken, *Beyond the Standard Model*, 5, 2010 [1005.1676].

[3] L. Canetti, M. Drewes and M. Shaposhnikov, *Matter and Antimatter in the Universe*, *New J. Phys.* **14** (2012) 095012 [1204.4186].

[4] V. Barger, D. Marfatia and K. Whisnant, *The physics of neutrinos*, Princeton Univ. Pr., Princeton, USA (2012).

[5] E. Corbelli and P. Salucci, *The Extended Rotation Curve and the Dark Matter Halo of M33*, *Mon. Not. Roy. Astron. Soc.* **311** (2000) 441 [astro-ph/9909252].

[6] N. Jarosik, C.L. Bennett, J. Dunkley, B. Gold, M.R. Greason, M. Halpern et al., *Seven-year wilkinson microwave anisotropy probe (wmap) observations: Sky maps, systematic errors, and basic results*, *The Astrophysical Journal Supplement Series* **192** (2011) 14.

[7] S. Weinberg, *Dreams of a final theory: The Search for the fundamental laws of nature* (1992).

[8] B. Holdom, *Two u(1)'s and epsilon charge shifts*, *Phys. Lett. B* **166** (1986) 196.

[9] M. Pospelov, *Secluded U(1) below the weak scale*, *Phys. Rev. D* **80** (2009) 095002 [0811.1030].

[10] A. Signer, *Low-energy Precision Physics and the High-energy Frontier*, *Phys. Procedia* **51** (2014) 25.

[11] M. Raggi and V. Kozhuharov, *Proposal to Search for a Dark Photon in Positron on Target Collisions at DAΦNE Linac*, *Adv. High Energy Phys.* **2014** (2014) 959802 [1403.3041].

[12] I.C. Brock et al., *Luminosity Measurement in the L3 Detector at LEP*, *Nucl. Instrum. Meth. A* **381** (1996) 236.

[13] M.D. Schwartz, *Quantum Field Theory and the Standard Model*, Cambridge University Press (3, 2014).

[14] M.E. Peskin and D.V. Schroeder, *An introduction to quantum field theory*, Westview, Boulder, CO (1995).

[15] P. Nogueira, *Automatic Feynman graph generation*, *J. Comput. Phys.* **105** (1993) 279.

[16] H.H. Patel, *Package-X: A Mathematica package for the analytic calculation of one-loop integrals*, *Comput. Phys. Commun.* **197** (2015) 276 [1503.01469].

[17] T. Engel, A. Signer and Y. Ulrich, *A subtraction scheme for massive QED*, *JHEP* **01** (2020) 085 [1909.10244].

[18] P. Banerjee, T. Engel, A. Signer and Y. Ulrich, *Qed at nnlo with mcmule*, arXiv:2007.01654.

[19] G.P. Lepage, *VEGAS: AN ADAPTIVE MULTIDIMENSIONAL INTEGRATION PROGRAM*, .

[20] Y. Ulrich, *McMule – QED Corrections for Low-Energy Experiments*, other thesis, 8, 2020, [2008.09383].

[21] L. Naterop, "Analytical results for master thesis, https://gitlab.com/lucanaterop/thesis-results."

[22] T. Becher and M. Neubert, *On the Structure of Infrared Singularities of Gauge-Theory Amplitudes*, *JHEP* **06** (2009) 081 [0903.1126].

[23] A. Mitov and S. Moch, *The Singular behavior of massive QCD amplitudes*, *JHEP* **05** (2007) 001 [hep-ph/0612149].

[24] C.W. Bauer, S. Fleming, D. Pirjol and I.W. Stewart, *An effective field theory for collinear and soft gluons: heavy to light decays*, arXiv:hep-ph/0011336.

[25] C.W. Bauer, D. Pirjol and I.W. Stewart, *Soft collinear factorization in effective field theory*, *Phys. Rev. D* **65** (2002) 054022 [hep-ph/0109045].

[26] M. Beneke, A.P. Chapovsky, M. Diehl and T. Feldmann, *Soft collinear effective theory and heavy to light currents beyond leading power*, *Nucl. Phys. B* **643** (2002) 431 [hep-ph/0206152].

[27] T. Becher and K. Melnikov, *Two-loop qed corrections to bhabha scattering*, arXiv:0704.3582.

[28] T. Liu, A.A. Penin and N. Zerf, *Three-loop quark form factor at high energy: the leading mass corrections*, *Phys. Lett. B* **771** (2017) 492 [1705.07910].

[29] T. Liu and A. Penin, *High-Energy Limit of Mass-Suppressed Amplitudes in Gauge Theories*, *JHEP* **11** (2018) 158 [1809.04950].

[30] T. Engel, C. Gnendiger, A. Signer and Y. Ulrich, *Small-mass effects in heavy-to-light form factors*, *JHEP* **02** (2019) 118 [1811.06461].

[31] C. Anastasiou, E.W.N. Glover and M.E. Tejeda-Yeomans, *Two loop QED and QCD corrections to massless fermion boson scattering*, *Nucl. Phys. B* **629** (2002) 255 [hep-ph/0201274].

[32] G. Passarino and M.J.G. Veltman, *One Loop Corrections for e+ e- Annihilation Into mu+ mu- in the Weinberg Model*, *Nucl. Phys. B* **160** (1979) 151.

[33] T. Engel, *"Two-loop corrections to the muon decay"*, Master's thesis, Swiss Federal Institute of Technology in Zurich, 2018.

[34] P. Valtancoli, *The scalar box integral and the mellin - barnes representation*, arXiv:1104.2661.

[35] T. Huber and D. Maître, *Hypexp 2, expanding hypergeometric functions about half-integer parameters*, arXiv:0708.2443.

[36] C. Gnendiger, A. Signer, D. Stöckinger, A. Broggio, A.L. Cherchiglia, F. Driencourt-Mangin et al., *To d, or not to d: Recent developments and comparisons of regularization schemes*, arXiv:1705.01827.

[37] E. Gardi and L. Magnea, *Factorization constraints for soft anomalous dimensions in qcd scattering amplitudes*, arXiv:0901.1091.

[38] E. Gardi and L. Magnea, *Infrared singularities in qcd amplitudes*, arXiv:0908.3273.

[39] T. Becher and M. Neubert, *Infrared singularities of scattering amplitudes in perturbative qcd*, arXiv:0901.0722.

[40] T. Becher and M. Neubert, *On the Structure of Infrared Singularities of Gauge-Theory Amplitudes*, *JHEP* **06** (2009) 081 [0903.1126].

[41] M. Jamin and M.E. Lautenbacher, *Tracer version 1.1: A mathematica package for γ-algebra in arbitrary dimensions*, *Computer Physics Communications* **74** (1993) 265.

[42] F. Buccioni, J.-N. Lang, J.M. Lindert, P. Maierhöfer, S. Pozzorini, H. Zhang et al., *Openloops 2*, arXiv:1907.13071.

[43] F. Cascioli, P. Maierhöfer and S. Pozzorini, *Scattering amplitudes with open loops*, *Phys. Rev. Lett.* **108** (2012) 111601.

[44] Buccioni, Federico, Pozzorini, Stefano and Zoller, Max, *On-the-fly reduction of open loops*, *Eur. Phys. J. C* **78** (2018) 70.

[45] M.J. Levine and R. Roskies, *New technique for vertex graphs*, *Phys. Rev. Lett.* **30** (1973) 772.

[46] M.J. Levine and R. Roskies, *Hyperspherical approach to quantum electrodynamics: sixth-order magnetic moment*, *Phys. Rev. D* **9** (1974) 421.

[47] S. Laporta and E. Remiddi, *The Analytic value of the light-light vertex graph contributions to the electron (g-2) in QED*, *Phys. Lett. B* **265** (1991) 182.

[48] L. Durand, *Pionic contributions to the magnetic moment of the muon*, *Phys. Rev.* **128** (1962) 441.

[49] J.H. Kuhn and S. Uccirati, *Two-loop QED hadronic corrections to Bhabha scattering*, *Nucl. Phys. B* **806** (2009) 300 [0807.1284].

[50] M. Fael, *Hadronic corrections to μ-e scattering at NNLO with space-like data*, *JHEP* **02** (2019) 027 [1808.08233].

[51] H.H. Patel, "PVReduce."

[52] S. Laporta, *Hyperspherical integration and the triple cross vertex graphs*, *Nuovo Cim. A* **107** (1994) 1729 [hep-ph/9404203].

[53] T. Kinoshita, *Mass singularities of Feynman amplitudes*, *J. Math. Phys.* **3** (1962) 650.

[54] T.D. Lee and M. Nauenberg, *Degenerate Systems and Mass Singularities*, *Phys. Rev.* **133** (1964) B1549.

[55] R.N. Lee, *Electron-positron annihilation to photons at $O(\alpha^3)$ revisited*, *Nucl. Phys. B* **960** (2020) 115200 [2006.11082].

[56] S. Frixione, Z. Kunszt and A. Signer, *Three jet cross-sections to next-to-leading order*, *Nucl. Phys. B* **467** (1996) 399 [hep-ph/9512328].

[57] D.R. Yennie, S.C. Frautschi and H. Suura, *The infrared divergence phenomena and high-energy processes*, *Annals Phys.* **13** (1961) 379.

[58] G. Balossini, C. Bignamini, C.M.C. Calame, G. Montagna, O. Nicrosini and F. Piccinini, *Photon pair production at flavour factories with per mille accuracy*, arXiv:0801.3360.

[59] T. Aoyama et al., *The anomalous magnetic moment of the muon in the Standard Model*, *Phys. Rept.* **887** (2020) 1 [2006.04822].

[60] F. Caola, A. von Manteuffel and L. Tancredi, *Di-photon amplitudes in three-loop quantum chromodynamics*, arXiv:2011.13946.

[61] B. Agarwal, F. Buccioni, A. von Manteuffel and L. Tancredi, *Two-loop leading colour QCD corrections to $q\bar{q} \to \gamma\gamma g$ and $qg \to \gamma\gamma q$*, *JHEP* **04** (2021) 201 [2102.01820].

A On-shell renormalization constants

In plain QED,

$$\delta_m = -\Sigma_0(\not{p})|_{\not{p}=m} = -\frac{\alpha}{4\pi}\frac{\Gamma(\epsilon+1)}{\epsilon}\left(\frac{4\pi\mu^2}{m^2}\right)^{\epsilon}\frac{3-2\epsilon}{1-2\epsilon} \tag{A.1}$$

$$\delta_1 = \delta_2 = \frac{d\Sigma_0(\not{p})}{d\not{p}}|_{\not{p}=m} = -\frac{\alpha}{4\pi}\frac{\Gamma(\epsilon+1)}{\epsilon}\left(\frac{4\pi\mu^2}{m^2}\right)^{\epsilon}\frac{3-2\epsilon}{1-2\epsilon} = \delta_m \tag{A.2}$$

where δ_2 contains contributions from UV and (soft) IR singularities.
If instead we choose to regularize the soft divergence in $\Sigma_0(\not{p})$ with a photon mass λ we find up to $\mathcal{O}(\epsilon^0)$

$$\delta_m = -\Sigma_0(\not{p})|_{\not{p}=m} = -\frac{3\alpha m}{4\pi\epsilon} - \frac{\alpha\left(2m^2\left(\lambda^2+3m^2\log\left(\frac{4\pi\mu^2}{m^2}\right)+4m^2\right)+\lambda^4\log\left(\frac{m^2}{\lambda^2}\right)+2\lambda\sqrt{\lambda^2-4m^2}\left(\lambda^2+2m^2\right)\log\left(\frac{\lambda+\sqrt{\lambda^2-4m^2}}{2m}\right)\right)}{8\pi m^3} \tag{A.3}$$

$$\begin{aligned}\delta_1 = \delta_2 = \frac{d\Sigma_0(\not{p})}{d\not{p}}|_{\not{p}=m} = &-\frac{\alpha}{4\pi\epsilon}+\frac{\alpha\left(-3\lambda^2-4m^2\right)}{4\pi m^2}-\frac{\alpha\left(4m^4-3\lambda^4\right)\log\left(\frac{\lambda^2}{m^2}\right)}{8\pi m^4}\\ &+\frac{3\alpha\sqrt{\lambda^4-4\lambda^2m^2}\left(\lambda^4-2\lambda^2m^2-4m^4\right)\log\left(\frac{\lambda^2+\sqrt{\lambda^4-4\lambda^2m^2}}{2\lambda m}\right)}{4\pi m^4\left(4m^2-\lambda^2\right)}-\frac{\alpha\log\left(\frac{4\pi\mu^2}{m^2}\right)}{4\pi}\end{aligned} \tag{A.4}$$

In the hyperspherical method, after performing the angular integration we obtain renormalization constants with residual Q^2 dependence

$$\delta_m = -\Sigma_0(\not{p})|_{\not{p}=m} = \frac{i\pi^2e^2\left(\sqrt{Q^2\left(4m^2+Q^2\right)}-Q^2\right)\left(\sqrt{Q^2\left(4m^2+Q^2\right)}+4m^2-Q^2\right)}{2m^3Q^4} \tag{A.5}$$

$$\begin{aligned}\delta_1 = \delta_2 &= \frac{d\Sigma_0(\not{p})}{d\not{p}}|_{\not{p}=m}\\ &= \frac{i\pi^2e^2\left(-4m^4\left(\sqrt{Q^2\left(4m^2+Q^2\right)}-3Q^2\right)-6m^2Q^4+3Q^4\left(\sqrt{Q^2\left(4m^2+Q^2\right)}-Q^2\right)\right)}{m^4Q^4\sqrt{Q^2\left(4m^2+Q^2\right)}}\end{aligned} \tag{A.6}$$

where we left implicit the factor $iQ^2/2$ from the transformation to hyperspherical variables and the factor $1/(2\pi)^4$ from the loop measure.

B Independence of ξ_c at NLO

The ξ_c independence of the NLO cross section is demonstrated in Figure B.1.

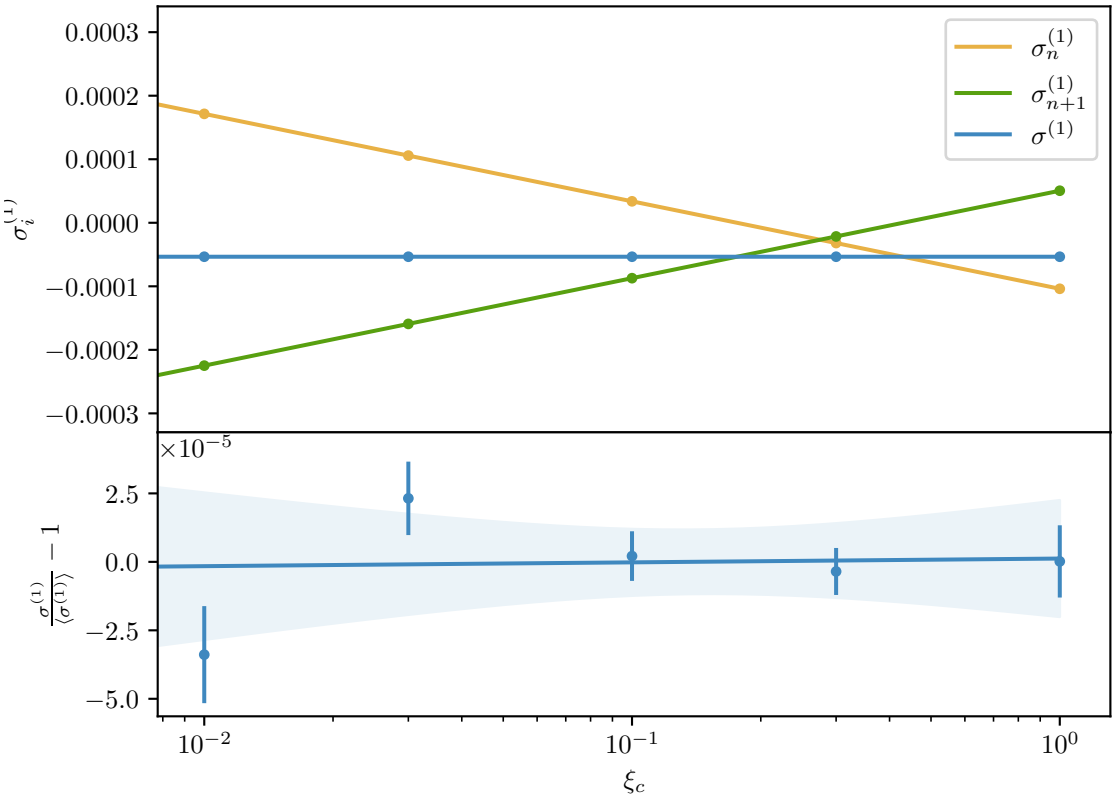

Figure B.1: Demonstration of ξ_c independence at NLO. Top: IR finite virtual, real and combined cross sections. Bottom: Linear fit and relative difference of $\sigma^{(1)}$ to fit with 2σ confidence displayed in shaded blue.